ChemComm
Chemical Communications

Accepted Manuscript

This article can be cited before page numbers have been issued, to do this please use: L. N. McHugh, M. F. Thorne, A. M. Chester, M. Etter, K. Užarevi and T. D. Bennett, *Chem. Commun.*, 2022, DOI: 10.1039/D2CC00278G.

ROYAL SOCIETY OF CHEMISTRY

rsc.li/chemcomm

View Article Online
DOI: 10.1039/D2CC00278G

COMMUNICATION

Mechanochemically Synthesised Dicyanamide Hybrid Organic-Inorganic Perovskites and their Melt-Quenched Glasses

Received 00th January 20xx,
Accepted 00th January 20xx

DOI: 10.1039/x0xx00000x

Lauren N. McHugh,[a] Michael F. Thorne,[a] Ashleigh M. Chester,[a] Martin Etter,[b] Krunoslav Užarević,[c] and Thomas D. Bennett*[a]

Here we present efficient and scalable mechanochemical formation of hybrid organic-inorganic perovskites of the form [TPrA][M(dca)$_3$] (M = Mn^{2+}, Co^{2+}) and the subsequent formation of their bulk melt-quenched glass samples. *In-situ* X-ray diffraction reveals direct, facile, and almost instantaneouos formation of both crystalline materials upon milling, while slow cooling limits recrystallisation in glass samples. The glasses show good stability to both acidic and basic aqueous solutions and display higher carbon dioxide uptakes than their crystalline precursors.

Hybrid organic-inorganic perovskites (HOIPs) with the formula ABX$_3$ (A = organic cation, B = metal cation and X = anion) are highly important materials within the field of materials science and display characteristics from both metal–organic frameworks (MOFs) and the parent perovskite family.[1] HOIPs have attracted considerable attention due to their multiferroic properties,[2] and their use as semiconductors[3] and photovoltaics.[4,5] The inclusion of anionic bridging ligands on the X-site such as formate [HCOO$^-$],[6] hypophosphite [$H_2PO_2^-$],[7] or dicyanamide (dca, [$C_2N_3^-$]),[8,9] further expand the structural diversity and functionality of this family.

In addition to the previously reported melting of 2D-layered HOIP series such as [(BA)$_2$MI$_4$] (BA = butylammonium [$C_4H_{12}N^+$], M = Ge^{2+}, Sn^{2+}, Pb^{2+}),[10] and [(AA)$_2$PbI$_4$] (AA = alkylammonium),[11] HOIPs with composition [TPrA][[M(dca)$_3$] (TPrA = tetrapropylammonium [$C_{12}H_{28}N^+$], M = Mn^{2+}, Co^{2+} and Fe^{2+}) were very recently shown to melt at *ca.* 250 °C. Upon cooling from the liquid state, glass analogues were produced, which displayed interesting thermal and electrical properties.[12] These, along with glasses formed from zeolitic imidazolate frameworks (ZIFs), both belong to the hybrid glass family, though the latter melt at higher temperatures of *ca.* 400 °C.[13] ZIF glasses show promising optical and mechanical properties,[14,15] and potential in applications including gas separation and battery technology.[16,17]

Mechanochemical synthesis involves solvent-free grinding to induce a chemical reaction and has been utilised for the green and efficient formation of several families of hybrid materials, mostly coordination polymers and MOFs.[18,19] Until now, only the most conventional HOIPs with composition MAPbI$_3$ (MA = methylammonium [CH_6N^+]) and similar mixed cation species with the general formula [(MA)$_x$(FA)$_{1-x}$PbI$_3$], (FA = formamidinium [$CH_5N_2^+$]) have been synthesised this way.[20,21]

HOIPs are predominantly prepared by slow crystallisation from layered solutions over several weeks.[8,9] Such techniques are somewhat inefficient and commonly rely on the use of high-vapour-pressure organic solvents, resulting in energy-consuming work-ups and the production of organic solvent waste. This long and costly processing, in turn, impacts the availability and potential cost of HOIP-based materials, such as their glasses, particularly on larger scales. The lower melting temperatures (T_ms) of HOIPs mean that processing into the bulk scale is, in theory, easier. Therefore, routes to increase the efficiency of and to scale-up the synthesis of the crystalline precursors are actively sought.

Here we present the first mechanochemical synthesis of HOIPs of the form [TPrA][[M(dca)$_3$] as a rapid, green and efficient method for producing perovskite materials and the subsequent formation of their melt-quenched glasses on a larger scale. Two members of the [TPrA][M(dca)$_3$] family of HOIPs: [TPrA][Mn(dca)$_3$],[8] and [TPrA][Co(dca)$_3$][9] were studied in this work. [TPrA][Mn(dca)$_3$] forms in the tetragonal space group $P\bar{4}2_1c$, while [TPrA][Co(dca)$_3$] forms in the orthorhombic space group *Pnna*. Both structures contain bridging dca ligands, which bind through the N atoms to the transition metal cations (**Figure 1a inset**).

In a typical mechanochemical experiment, crystalline HOIP samples were formed after 30 minutes of milling (**see methods**), where the quantity of the liquid additive was optimised for the

[a] *Department of Materials Science and Metallurgy, University of Cambridge, 27 Charles Babbage Road, Cambridge, Cambridgeshire, CB3 0FS.*
[b] *Deutsches Elektronen Synchrotron, FS-PETRA-D, P02.1, Notkestr. 85, 22607 Hamburg, Germany.*
[c] *Ruđer Bošković Institute, Zagreb, Croatia.*
E-mail: tdb35@cam.ac.uk
† Electronic Supplementary Information (ESI) available. See
DOI: 10.1039/x0xx00000x

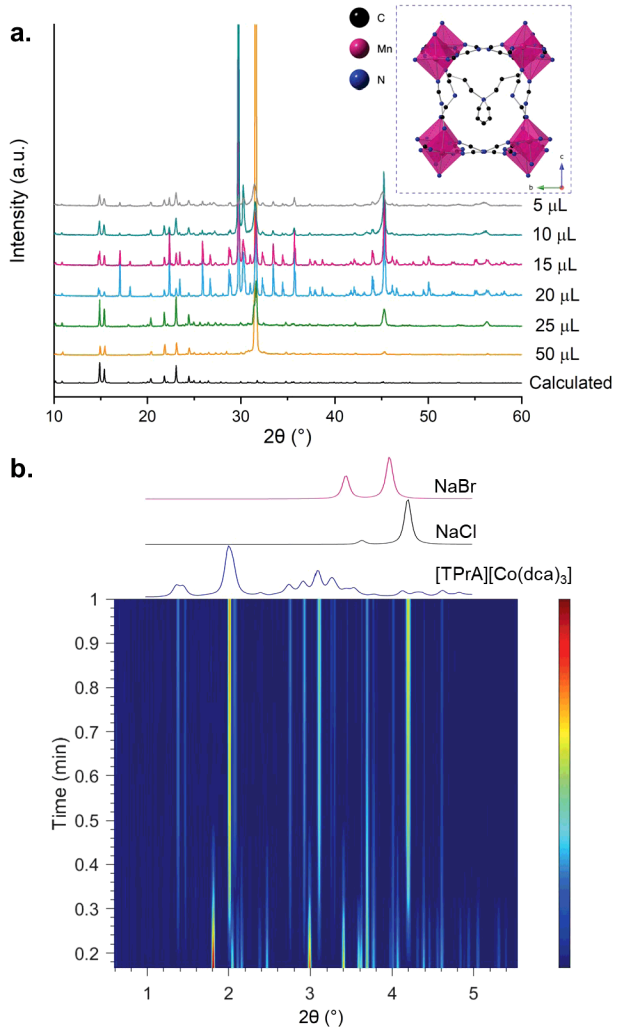

Figure 1a. PXRD patterns of unwashed [TPrA][Mn(dca)$_3$] using different quantities of a 2:1 H_2O:EtOH solvent mixture. 25 µL was chosen for subsequent syntheses after comparison with the calculated trace. **Inset.** Simplified structure of [TPrA][Mn(dca)$_3$], showing one of the possible orientations within the average crystal structure.[8] H atoms have been omitted for clarity and only the TPrA ion located on the body-centre position is visible. **b.** *In-situ* PXRD of [TPrA][Co(dca)$_3$], showing that the material forms after *ca.* 30 seconds Red = areas of high intensity and blue = areas of low intensity. Simulated PXRD patterns of [TPrA][Co(dca)$_3$], NaCl and NaBr are shown for clarity.

smaller-scale synthesis of [TPrA][Mn(dca)$_3$] (**Figure 1a**). Attempted mechanochemical formation of [TPrA][Fe(dca)$_3$] was ultimately unsuccessful (**Figure S1**) and it was chosen to focus on the manganese and cobalt examples only. While the mechanochemical syntheses were highly efficient, larger-scale samples were required to conduct further analysis, therefore a larger milling jar was utilised to scale-up production fivefold. This method was highly successful and did not require any alterations to reagent or solvent ratios. Further analyses in this study were performed on samples produced on a larger-scale. Samples were initially formed containing sodium chloride and sodium bromide salt by-products (**Figure S2, S3**), which were readily removed by washing with ice-cold distilled water (**Figures S4 and S5**). The mechanochemical formation of both [TPrA][Mn(dca)$_3$] and [TPrA][Co(dca)$_3$] was monitored using *in-situ* synchrotron PXRD (**see methods**).[22] [TPrA][Mn(dca)$_3$] forms directly within 10 minutes (**Figure S6**), whereas [TPrA][Co(dca)$_3$] formed almost immediately, in under 1 minute of milling (**Figure 1b**, **Figure S7**). These facile and efficient, laboratory-scale mechanosyntheses demonstrate the potential for further scale-up, or continuous synthesis using extrusion.[23]

Thermogravimetric analysis (TGA) was performed under both argon (Ar) and nitrogen (N_2) on [TPrA][Mn(dca)$_3$] (**Figure S8, S9**) and [TPrA][Co(dca)$_3$] (**Figure S10, S11**) prior to differential scanning calorimetry (DSC) (**Figure 2**), where the samples were heated, cooled, then heated again under Ar, using a heating/cooling rate of 10 °C min^{-1}. Significant recrystallisation was observed for [TPrA][Mn(dca)$_3$] (**Figure S12**) and the glass transition temperature (T_g) was situated close to the second melting peak. This is likely due to the sample beginning to decompose immediately after melting. [TPrA][Mn(dca)$_3$] was then cooled at 3 °C min^{-1} (**Figure S13**) in an attempt to reduce the extent of recrystallisation upon cooling, which was ultimately successful. The sample showed little to no recrystallisation on the cooling step, and a T_g was again evident. Comparable DSC analysis was performed on [TPrA][Co(dca)$_3$], where one sample was heated, cooled and heated at a rate of 10 °C min^{-1} (**Figure S14**), while another was cooled at 3 °C min^{-1} (**Figure S15**). Cooling at a slower rate again reduced the extent of recrystallisation, and a T_g was observed for the sample cooled at 10 °C min^{-1}, though not for the sample cooled at 3 °C min^{-1}. The mechanochemically synthesised samples both melted at lower temperatures than those produced by slow crystallisation (**Table S1**), likely due to the significantly lower particle size of mechanochemically produced samples. Similar behaviour has been observed in nanoscale materials.[24] Mechanochemical samples also displayed lower decomposition temperatures (T_ds) than traditionally synthesised HOIPs (**Table S1**) and the T_gs for both were higher than those reported in literature (**Table S1**). Low-temperature DSC was also performed under N_2 (**Figure S16, S17**), where samples were heated to the desired temperature, cooled to -60 °C, then heated again. Both displayed broadly comparable T_ms and T_gs to those under Ar (**Table S1**).

HOIP glass samples produced by Shaw et al.[12] were formed on a small-scale inside an SDT (simultaneous TGA-DSC) furnace, which limited batches to *ca.* 15 mg. SDT was also used here to investigate the optimum temperature and heating/cooling rate to minimise recrystallisation in samples, where samples were

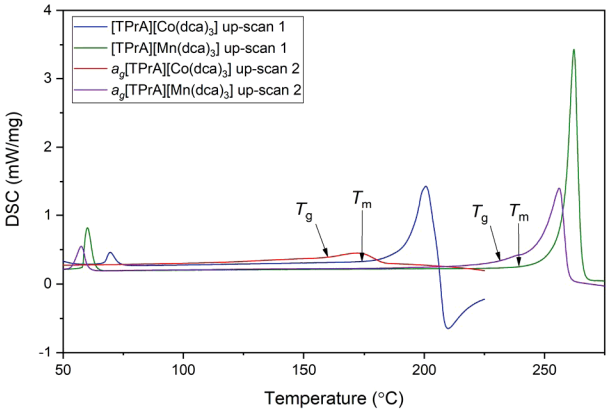

Figure 2. DSC traces of [TPrA][Co(dca)$_3$] and [TPrA][Mn(dca)$_3$], showing the first and second up-scans recorded at a heating rate of 10 °C min^{-1}. The T_m and T_g are shown for each sample and a_g denotes the glass-phase. A second melting peak is observed close to the T_g for a_g[TPrA][Mn(dca)$_3$] due to significant recrystallisation within the sample upon cooling. The endothermic features at *ca.* 50-70 °C represent previously reported solid-solid phase transitions.[8,9]

heated to close to their T_d to minimise recrystallisation. The samples were heated at 10 °C min^{-1}, before being cooled at either 10 °C min^{-1} or 3 °C min^{-1} (**Figures S18-S21**). In agreement with previous DSC analysis, considerable recrystallisation was observed in a_g[TPrA][Mn(dca)$_3$] upon cooling at 10 °C min^{-1}, while cooling at 3 °C min^{-1} lead to a fully amorphous sample (**Figure S22).** No recrystallisation to the original phase was observed for a_g[TPrA][Co(dca)$_3$] upon cooling at 10 °C min^{-1} or the slower rate of 3 °C min^{-1}, regardless of the cooling rate (**Figure S23**). However, some extremely minor Bragg peaks, attributed to impurities, were observed in the sample cooled at 3 °C min^{-1}.

To produce bulk glass samples, crystalline HOIPs were heated to 260 °C for [TPrA][Mn(dca)$_3$] and 240 °C for [TPrA][Co(dca)$_3$] within a tube furnace and under flowing Ar. The sample was then cooled to room temperature naturally over several hours. Very minor oxidation was evident in both glass samples at *ca.* 45°, though no recrystallisation was observed for either (**Figure S24**). From previous analysis, it appeared that slow cooling of samples, especially [TPrA][Mn(dca)$_3$], helped limit recrystallisation. This is somewhat contradictory to traditional glasses, where rapid cooling of the melt is typically required for glass formation.[25] In glasses derived from HOIPs, there appears to be a complex interplay between glass-formation, decomposition and recrystallisation. With slower cooling, HOIP samples are held at close to their T_d for extended periods, which leads to minor sample decomposition and reduced likelihood of a return to the original, ordered crystalline state. This degree of sample decomposition is evident from CHN microanalysis (**Table S2**), where compositional changes were observed upon glass formation for both [TPrA][Mn(dca)$_3$] and [TPrA][Co(dca)$_3$]. The larger compositional differences observed between [TPrA][Mn(dca)$_3$] and a_g[TPrA][Mn(dca)$_3$] are likely due to the relatively small melting window prior to decomposition.

The initial crystalline sample [TPrA][Mn(dca)$_3$] consisted of block-like crystals (**Figure S25a, b**), which appeared to flow together upon glass-formation to give a material with clear surface porosity (**Figure S25c, d**). Similarly, crystalline [TPrA][Co(dca)$_3$] also consisted of rounded 'blocky' crystals (**Figure S26a, b**). The sample also appeared to have undergone significant flow upon glass-formation, to provide a relatively smooth material with minor surface porosity (**Figure S26c, d**).

Crystalline and glass samples of [TPrA][Mn(dca)$_3$] and [TPrA][Co(dca)$_3$] were exposed to acidic, neutral or basic conditions (**see methods**) to assess the effect of pH on the chemical stability of HOIPs and their glasses. Similar studies have been performed on both inorganic and MOF glasses to determine their stabilities.[26,27] a_g[TPrA][Mn(dca)$_3$] appeared stable from PXRD in solutions with pH 2, 5, 7 and 10, with no recrystallisation to the original crystalline phase, though very minor impurity peaks were present (**Figure S27**). a_g[TPrA][Co(dca)$_3$] also appeared stable from PXRD in strongly acidic, mildly acidic, neutral and mildly basic solutions, with no evidence of recrystallisation (**Figure S28**). Some changes in composition were observed in glass samples exposed to aqueous solutions when compared to the initial glass samples (**Table S2**), where CHN microanalysis showed appreciable reductions in the carbon and hydrogen weight percentages. These differences may be attributed to minor hydrolysis of glass samples, leading to the presence of oxygen atoms which cannot be seen via CHN analysis. This therefore affects the composition and skews the percentages of C, H and N. It is important to note, however, that the percentage compositions of C, H and N in recovered glass samples remained somewhat consistent, regardless of the strength of the acidic or basic solution. Most crystalline samples dissolved in solutions regardless of pH, though like the glasses, crystalline samples of unknown origin were recovered solely from strongly basic solutions (pH 13, **Figure S29, S30**). These stability differences reflect the different local structure present in the crystalline and glass samples.

Pellets of both crystalline and glass samples were synthesised (**see methods**) (**Figures S31** and **S32**). Optical microscopy of the glass pellets highlighted the significant differences in the form of the materials upon heating, where a_g[TPrA][Co(dca)$_3$] formed as a mostly flat pellet with an almost pearlescent appearance (**Figure S33a**). However, the a_g[TPrA][Mn(dca)$_3$] pellet expanded vertically to form a stratified sample with surface cracks (**Figure S33b**).

The hydrophobicity of pelletised a_g[TPrA][Co(dca)$_3$] was investigated using water contact angle measurements (**see methods**, **Figure S34**). The glass surface was found to be fairly hydrophilic, with a mean water contact angle of 57.53 ± 1.38°. Measurements were not attempted on a_g[TPrA][Mn(dca)$_3$] due to the very fragile pellet, which fragmented upon handling.

HOIPs are typically non-porous materials and consequently, gas adsorption is not normally performed. Shaw et al. proposed that the melting mechanism in [TPrA][M(dca)$_3$] HOIPs involved the movement of the TPrA cation, leading to a large structural change. Gas adsorption measurements were subsequently performed to investigate whether this change in conformation upon melt-quenching may introduce a degree of porosity into the samples. It is known that N_2 gas cannot enter micropores with a width of less than 4.5 Å due to kinetic restrictions,[28] and as HOIPs are usually non-porous, the smaller kinetic diameter CO_2 molecule was used as an analyte in this study to maximise the likelihood of adsorption. The CO_2 adsorption isotherms for the crystalline and glass forms of [TPrA][Mn(dca)$_3$] and [TPrA][Co(dca)$_3$] are shown in **Figures 3a** and **3b** respectively, where CO_2 uptakes were recorded up to a relative pressure of 0.035 P/P_0. [TPrA][Mn(dca)$_3$] and [TPrA][Co(dca)$_3$] provided CO_2 uptake values of 3.44 cm^3 g^{-1} and 3.22 cm^3 g^{-1} respectively, where the very low levels of adsorption highlighted the non-porous nature of the crystalline HOIPs. a_g[TPrA][Mn(dca)$_3$] and a_g[TPrA][Co(dca)$_3$] afforded CO_2 uptake values of 14.90 cm^3 g^{-1} and 9.00 cm^3 g^{-1} respectively, and though they are still not considered particularly porous, the CO_2 capacities were considerably higher than their crystalline counterparts. This is especially true for a_g[TPrA][Mn(dca)$_3$], where the CO_2 uptake increased by a factor of 4 upon glass formation. The shapes of the isotherms also changed upon glass formation. Whereas the change was minor for a_g[TPrA][Co(dca)$_3$], the isotherm of a_g[TPrA][Mn(dca)$_3$] more closely resembled that of a type I isotherm-indicative of a microporous material such as a MOF. This may be due to the greater extent of surface porosity visible

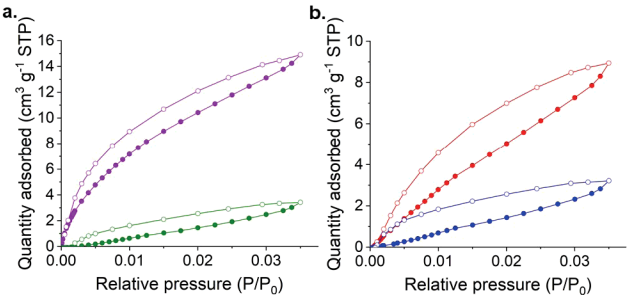

Figure 3. Carbon dioxide adsorption isotherms recorded for **a.** [TPrA][Mn(dca)$_3$] (green trace) and a_g[TPrA][Mn(dca)$_3$] (purple trace), **b.** [TPrA][Co(dca)$_3$] (blue trace) and a_g[TPrA][Co(dca)$_3$] (red trace). Closed circles represent adsorption points and open circles represent desorption points.

in a_g[TPrA][Mn(dca)$_3$] when compared to a_g[TPrA][Co(dca)$_3$]. The significant increase in gas uptake in the glass forms compared to their crystalline counterparts is consistent with the large structural change upon melting previously proposed.

In this work, we have shown the mechanochemical synthesis of the HOIPs [TPrA][Mn(dca)$_3$] and [TPrA][Co(dca)$_3$] and the subsequent formation of bulk samples of their glass forms. Mechanochemical synthesis was used as an alternative to traditional slow-crystallisation and offered a green, rapid and scalable synthetic route to dicyanamide HOIPs of the form [TPrA][M(dca)$_3$]. Bulk samples of a_g[TPrA][Mn(dca)$_3$] and a_g[TPrA][Co(dca)$_3$] were formed in a standard tube furnace and the glasses showed good stability to all except strongly basic aqueous solutions. a_g[TPrA][Co(dca)$_3$] displayed moderate hydrophilicity, with a mean water contact angle of 57.53 ± 1.38°. The CO_2 uptakes of the HOIP glasses were higher than those of the corresponding non-porous crystalline samples, suggesting a significant structural change upon glass formation, such as the movement of A-site TPrA cations suggested in prior literature. Given the promising thermoelectric properties previously investigated for the glasses, the scalable synthesis of the materials may promote their applicability in real-world applications.

This work was financially supported by a Royal Society URF (UF150021) and research grant (RSG\R1\180395), a Philip Leverhulme Prize (2019) and the "Research Cooperability" Program of the Croatian Science Foundation funded by the European Union from the European Social Fund under the Operational Programme Efficient Human Resources 2014-2020, through grant PZS-2019-02-4129. *In-situ* PXRD was performed at the Deutsches Elektronen-Synchrotron PETRA III beamline P02.1. We wish to thank Dr. Ivana Brekalo for assistance with data collection and Dr. Stipe Lukin for help in data analysis.

Conflicts of interest

There are no conflicts to declare.

Notes and references

1 W. Li, Z. Wang, F. Deschler, S. Gao, R. H. Friend and A. K. Cheetham, *Nat. Rev. Mater.*, 2017, **2**, 16099.
2 Y. Tian, A. Stroppa, Y. Chai, L. Yan, S. Wang, P. Barone, S. Picozzi and Y. Sun, *Sci. Rep.*, 2014, **4**, 1–5.
3 T. M. Brenner, D. A. Egger, L. Kronik, G. Hodes and D. Cahen, *Nat. Rev. Mater.*, 2016, **1**, 1–16.
4 M. M. Lee, J. Teuscher, T. Miyasaka, T. N. Murakami and H. J. Snaith, *Science*, 2012, **338**, 643–647.
5 B. Zhao, S. Bai, V. Kim, R. Lamboll, R. Shivanna, F. Auras, J. M. Richter, L. Yang, L. Dai, M. Alsari, X. J. She, L. Liang, J. Zhang, S. Lilliu, P. Gao, H. J. Snaith, J. Wang, N. C. Greenham, R. H. Friend and D. Di, *Nat. Photonics*, 2018, **12**, 783–789.
6 P. Jain, V. Ramachandran, R. J. Clark, H. D. Zhou, B. H. Toby, N. S. Dalal, H. W. Kroto and A. K. Cheetham, *J. Am. Chem. Soc.*, 2009, **131**, 13625–13627.
7 Y. Wu, S. Shaker, F. Brivio, R. Murugavel, P. D. Bristowe and A. K. Cheetham, *J. Am. Chem. Soc.*, 2017, **139**, 16999–17002.
8 J. M. Bermúdez-García, M. Sánchez-Andújar, S. Yáñez-Vilar, S. Castro-García, R. Artiaga, J. López-Beceiro, L. Botana, Á. Alegría and M. A. Señarís-Rodríguez, *Inorg. Chem.*, 2015, **54**, 11680–11687.
9 J. M. Bermúdez-García, M. Sánchez-Andújar, S. Yáñez-Vilar, S. Castro-García, R. Artiaga, J. López-Beceiro, L. Botana, A. Alegría and M. A. Señarís-Rodríguez, *J. Mater. Chem. C*, 2016, **4**, 4889–4898.
10 D. B. Mitzi, *Chem. Mater.*, 1996, **8**, 791–800.
11 T. Li, W. A. Dunlap-Shohl, E. W. Reinheimer, P. Le Magueres and D. B. Mitzi, *Chem. Sci.*, 2019, **10**, 1168–1175.
12 B. K. Shaw, A. R. Hughes, M. Ducamp, S. Moss, A. Debnath, A. F. Sapnik, M. F. Thorne, L. N. McHugh, A. Pugliese, D. S. Keeble, P. Chater, J. M. Bermudez-Garcia, X. Moya, S. K. Saha, D. A. Keen, F. X. Coudert, F. Blanc and T. D. Bennett, *Nat. Chem.*, 2021, **13**, 778–785.
13 T. D. Bennett, Y. Yue, P. Li, A. Qiao, H. Tao, N. G. Greaves, T. Richards, G. I. Lampronti, S. A. T. Redfern, F. Blanc, O. K. Farha, J. T. Hupp, A. K. Cheetham and D. A. Keen, *J. Am. Chem. Soc.*, 2016, **138**, 3484–3492.
14 A. Qiao, H. Tao, M. P. Carson, S. W. Aldrich, L. M. Thirion, T. D. Bennett, J. C. Mauro and Y. Yue, *Opt. Lett.*, 2019, **44**, 1623.
15 S. Li, R. Limbach, L. Longley, A. A. Shirzadi, J. C. Walmsley, D. N. Johnstone, P. A. Midgley, L. Wondraczek and T. D. Bennett, *J. Am. Chem. Soc.*, 2019, **141**, 1027–1034.
16 Y. Wang, H. Jin, Q. Ma, K. Mo, H. Mao, A. Feldhoff, X. Cao, Y. Li, F. Pan and Z. Jiang, *Angew. Chemie - Int. Ed.*, 2020, **59**, 4365–4369.
17 G. Jiang, C. Qu, F. Xu, E. Zhang, Q. Lu, X. Cai, S. Hausdorf, H. Wang and S. Kaskel, *Adv. Funct. Mater.*, 2021, **31**, 2104300.
18 M. F. Thorne, M. L. R. Gómez, A. M. Bumstead, S. Li and T. D. Bennett, *Green Chem.*, 2020, **22**, 2505–2512.
19 T. Stolar and K. Užarević, *CrystEngComm*, 2020, **22**, 4511–4525.
20 D. Prochowicz, M. Franckevičius, A. M. Cieślak, S. M. Zakeeruddin, M. Grätzel and J. Lewiński, *J. Mater. Chem. A*, 2015, **3**, 20772–20777.
21 D. Prochowicz, P. Yadav, M. Saliba, M. Saski, S. M. Zakeeruddin, J. Lewiński and M. Grätzel, *Sustain. Energy Fuels*, 2017, **1**, 689–693.
22 K. Užarević, I. Halasz and T. Friščić, *J. Phys. Chem. Lett.*, 2015, **6**, 4129–4140.
23 D. Crawford, J. Casaban, R. Haydon, N. Giri, T. McNally and S. L. James, *Chem. Sci.*, 2015, **6**, 1645–1649.
24 J. Sun and S. L. Simon, *Thermochim. Acta*, 2007, **463**, 32–40.
25 B. Karmakar, *Fundamentals of Glass and Glass Nanocomposites*, Elsevier Inc., 2016.
26 A. Paul, *J. Mater. Sci.*, 1977, **12**, 2246–2268.
27 S. Li, S. Yu, S. M. Collins, D. N. Johnstone, C. W. Ashling, A. F. Sapnik, P. A. Chater, D. S. Keeble, L. N. McHugh, P. A. Midgley, D. A. Keen and T. D. Bennett, *Chem. Sci.*, 2020, **11**, 9910–9918.
28 K. A. Cychosz and M. Thommes, *Engineering*, 2018, **4**, 559–566.